

See discussions, stats, and author profiles for this publication at: <https://www.researchgate.net/publication/282344984>

# Dynamic Cross-Linking of Polymeric Binders Based on Host–Guest Interactions for Silicon Anodes in Lithium Ion Batteries

ARTICLE *in* ACS NANO · SEPTEMBER 2015

Impact Factor: 12.88 · DOI: 10.1021/acsnano.5b05030

---

READS

82

## 6 AUTHORS, INCLUDING:



[Erhan Deniz](#)

Qatar University

42 PUBLICATIONS 1,184 CITATIONS

[SEE PROFILE](#)



[Siham Alqaradawi](#)

Qatar University

33 PUBLICATIONS 338 CITATIONS

[SEE PROFILE](#)



[Jang Wook Choi](#)

Korea Advanced Institute of Science and Tec...

112 PUBLICATIONS 6,190 CITATIONS

[SEE PROFILE](#)



[Ali Coskun](#)

Korea Advanced Institute of Science and Tec...

64 PUBLICATIONS 3,124 CITATIONS

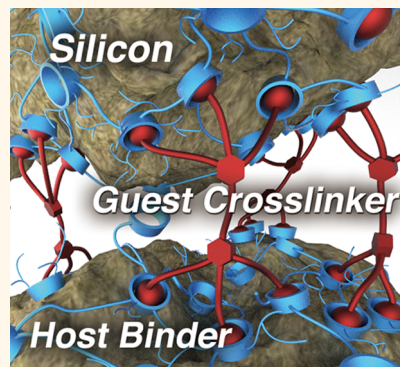
[SEE PROFILE](#)

# Dynamic Cross-Linking of Polymeric Binders Based on Host–Guest Interactions for Silicon Anodes in Lithium Ion Batteries

Tae-woo Kwon,<sup>†,II</sup> You Kyeong Jeong,<sup>†,II</sup> Erhan Deniz,<sup>§</sup> Siham Y. AlQaradawi,<sup>§</sup> Jang Wook Choi,<sup>\*,†</sup> and Ali Coskun<sup>\*,†,‡</sup>

<sup>†</sup>Graduate School of E�WS and KAIST Institute NanoCentury and <sup>‡</sup>Department of Chemistry, Korea Advanced Institute of Science and Technology (KAIST), Daejeon 305-701, Republic of Korea and <sup>§</sup>Department of Chemistry and Earth Sciences, College of Arts and Sciences, Qatar University, P.O. Box 2713, Doha, Qatar. <sup>II</sup>T.-w.K. and Y.K.J. equally contributed to this work.

**ABSTRACT** We report supramolecular cross-linking of polymer binders *via* dynamic host–guest interactions between hyperbranched  $\beta$ -cyclodextrin polymer and a dendritic gallic acid cross-linker incorporating six adamantane units for high-capacity silicon anodes. Calorimetric analysis in the solution phase indicates that the given host–guest complexation is a highly spontaneous and enthalpically driven process. These findings are further verified by carrying out gelation experiments in both aqueous and organic media. The dynamic cross-linking process enables intimate silicon–binder interaction, structural stability of electrode film, and controlled electrode–electrolyte interface, yielding enhanced cycling performance. Control experiments using both  $\alpha$ ,  $\gamma$ -CDp with different cavity sizes and a guest molecule incorporating a single adamantane unit verified that the enhanced cycle life originates from the host–guest interaction between  $\beta$ -cyclodextrin and adamantane. The impact of the dynamic cross-linking is maximized at an optimal stoichiometry between the two components. Importantly, the present investigation proves that the molecular-level tuning of the host–guest interactions can be translated directly to the cycling performance of silicon anodes.



**KEYWORDS:** binder · dynamic cross-linking · host–guest interaction · supramolecular chemistry · silicon anodes

## INTRODUCTION

The battery community has confronted an ever-growing demand to increase the energy densities of lithium ion batteries (LIBs) for the timely advent of advanced mobile electronics and electric vehicles. Silicon (Si) anodes are expected to play an important role in meeting this desperate demand by utilizing their unparalleled gravimetric capacities that surpass even 3000 mAh g<sup>-1</sup>.<sup>1</sup> Nonetheless, Si anodes suffer from insufficient cycle lives originating from tremendous volume expansion, indeed up to 300%. While a variety of electrode structures<sup>2–8</sup> and active phases<sup>9–13</sup> have been developed to mitigate unwanted shortcomings from the volume expansion, polymeric binder has turned out to be very critical in maintaining electrode structure and consequently initial capacity.<sup>14–17</sup>

Most conventional LIB electrodes, without undergoing large volume expansion, have adopted polyvinylidene difluoride (PVDF) as a binder due to its relatively good adhesion, electrochemical stability, reasonable cost, highly specific dielectric constant, and decent Li ion conductivity. However, PVDF showed very poor cycling performance for Si anodes pointing to the fact that conventional binders possessing only weak van der Waals interactions are not suitable for alloying active materials accompanying large volume expansions. Instead, several new binder concepts, namely, covalent cross-linking,<sup>18–20</sup> use of conductive polymers,<sup>21,22</sup> covalent attachment to Si,<sup>18–20,23</sup> hyperbranched polymer networks,<sup>24,25</sup> mussel- and millipede-inspired adhesion,<sup>26–28</sup> and self-healing,<sup>20,29,30</sup> have been lately introduced and shown to improve the electrochemical

\* Address correspondence to coskun@kaist.ac.kr, jangwookchoi@kaist.ac.kr.

Received for review August 12, 2015 and accepted September 30, 2015.

Published online  
10.1021/acsnano.5b05030

© XXXX American Chemical Society

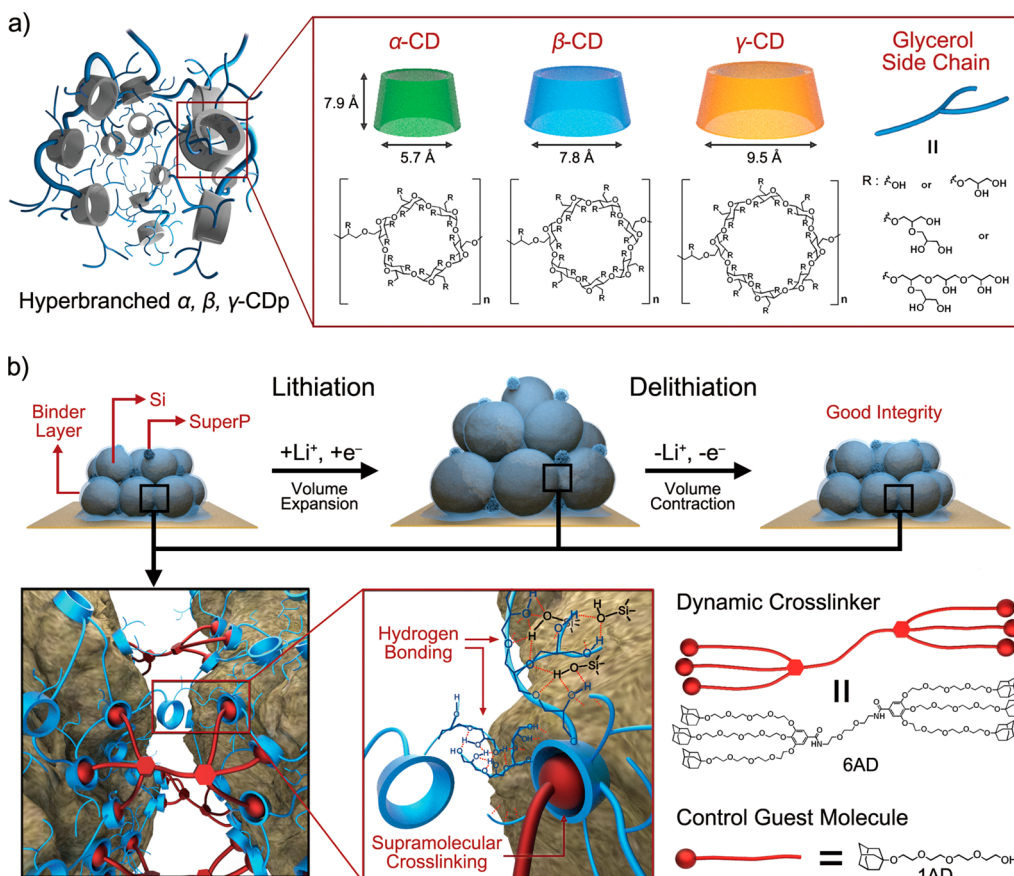


**Figure 1.** (a) Graphical representation and chemical structures of hyperbranched  $\alpha$ -,  $\beta$ -, and  $\gamma$ -CDp. (b) Proposed working mechanism of dynamic cross-linking of  $\beta$ -CDp and 6AD in an electrode matrix along with graphical representations and chemical structures of guest molecules incorporating adamantane moiety.

51 performance of Si anodes significantly. In particular,  
52 our recent systematic study revealed<sup>20</sup> that their self-  
53 healing capability is most effective for cycling perfor-  
54 mance by allowing recovery of Si–binder interactions  
55 that were lost during the volume expansion of Si,  
56 suggesting the useful nature of various supramolecular  
57 interactions (hydrogen bonding,  $\pi$ – $\pi$  stacking, ion–  
58 dipole interaction) in binder design for Si anodes.  
59 In a similar effort to enhance Si–binder interactions,  
60 covalent cross-linking is also actively pursued in the  
61 binder research. However, their structural stability  
62 under reductive potentials and limited elasticity to  
63 accommodate the volume change of Si are yet to be  
64 resolved.

65 Herein, we introduce an unconventional binder  
66 concept, “dynamic crosslinking”, for silicon nanoparti-  
67 cle anodes by engaging host–guest interactions be-  
68 tween hyperbranched  $\beta$ -cyclodextrin polymer ( $\beta$ -CDp)  
69 and a dendritic gallic acid derived supramolecular  
70 cross-linker incorporating six adamantane units. The  
71 dynamic cross-linking refers to a reversible cross-  
72 linking system based on host–guest interactions,  
73 which can restore broken linkages between polymer  
74 chains during continuous cycling. Unlike conventional  
75 covalent cross-linking, the reversibility of dynamic

cross-linking enables the homogeneous cross-linking  
76 between polymer chains, thus introducing a self-  
77 healing effect. The dynamic host–guest interactions  
78 effectively maintain the Si–binder interactions and,  
79 thus, the film integrity during repeated volume  
80 changes of Si, leading to a good cycling performance  
81 (90% capacity retention after 150 cycles with  $0.8 \text{ mg cm}^{-2}$   
82 Si loading). Control experiments using  $\alpha$ , $\gamma$ -CDp with  
83 different cavity sizes as well as a guest molecule  
84 incorporating single adamantane unit verified that  
85 the enhanced cycling performance arises solely from  
86 the designed host–guest interactions and resulting  
87 dynamic cross-linking.  
88

## RESULTS AND DISCUSSION

In order to demonstrate the dynamic cross-linking  
90 concept, we identified (Figure 1a) cyclodextrins (CDs)  
91 F1 as supramolecular hosts because (1) they can form  
92 strong inclusion complexes in an aqueous environ-  
93 ment with hydrophobic guests, (2) can be easily func-  
94 tionalized through primary and secondary alcohols  
95 located in each face, and (3) can be readily synthesized  
96 on a ton scale upon enzymatic degradation of starch.  
97 Cyclodextrins are macrocyclic oligosaccharides usually  
98 comprising six to eight (1,4)- $\alpha$ -D-glucopyranose units,  
99

namely,  $\alpha$ -CD,  $\beta$ -CD, and  $\gamma$ -CD with inner cavity diameters of 5.7, 7.8, and 9.50 Å, respectively. Orientation of glucopyranoside units renders the inner cavity of CDs hydrophobic, whereas hydrophilic —OH functionalities facilitate their water solubility, thus creating a unique size- and shape-selective complexation ability toward hydrophobic guest molecules in an aqueous medium. Interestingly, CDs can also bind<sup>31</sup> with substrates in polar aprotic solvents, such as DMSO with relatively high dielectric constant of 3.96 D. As previously shown by Breslow *et al.*,<sup>32</sup> the binding in nonaqueous media is mostly driven by lyophobic forces, which is similar to that in aqueous solution, arising from increased solvent—solvent interactions upon complexation. Although the binding constants were relatively lower compared to the ones in an aqueous solution, the rate of complexation was found to be much faster in non-aqueous media.

In order to utilize CDs as polymeric binders for silicon anodes, we used (Figure 1) hyperbranched cyclodextrin polymers, which can be easily obtained by reacting corresponding CDs with epichlorohydrin in water under basic conditions.<sup>33</sup> <sup>1</sup>H NMR analysis of the polymers (see Supporting Information, SI, Figures S1–S3) revealed that the resulting polymers contain comparable amounts of CD, which are 53, 51, and 52 wt % for  $\alpha$ -CDp,  $\beta$ -CDp, and  $\gamma$ -CDp, respectively. As for the guest molecule, we have chosen adamantane (AD) as an appropriate guest moiety due to its high affinity and selective binding to  $\beta$ -CD.<sup>34</sup> We have synthesized (see the SI, Figures S4–S8) and fully characterized a dendritic gallic acid derived guest molecule comprising six tetraethylene glycol substituted AD units (6AD) and a control guest composed of only one AD—tetraethylene glycol unit (1AD). The synthesis of 6AD was achieved in 83% yield by TBTU coupling of triadamantyl-terminated gallic acid with 2,2'-(ethylenedioxy)-bis(ethylamine) in DMF at 25 °C for 25 h.

In order to confirm the inclusion of a 1AD unit in  $\beta$ -CDp, we carried out (Figure 2) isothermal titration calorimetry (ITC) experiments in H<sub>2</sub>O at 298 K. For the ITC experiments, the exact concentration of  $\beta$ -CD units within  $\beta$ -CDp was obtained (see the SI) from <sup>1</sup>H NMR analysis. Thus, from the ITC analyses using 1AD as the guest molecule, the accessibility of  $\beta$ -CD units within the polymer network was determined and quantitatively understood. In the case of 6AD, an ITC experiment was not possible due to its relatively low solubility in water. Figure 2 shows exothermic heat flows released upon successive addition of  $\beta$ -CDp into the solution of 1AD in H<sub>2</sub>O at 298 K. Fitting the differential binding curve to the single-site binding model allowed us to directly determine  $K$ ,  $N$ ,  $\Delta H$ , and  $\Delta S$  values. Interestingly, the stoichiometry of binding,  $N$ , between 1AD and  $\beta$ -CDp was found to be 0.999, which is in perfect agreement with 1:1 stoichiometry. This result also indicates that all  $\beta$ -CD units within the

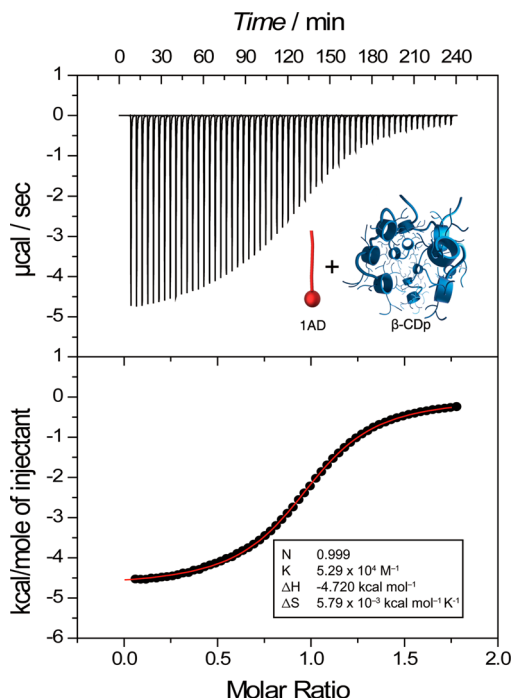


**Figure 2.** Binding isotherm of 1AD and  $\beta$ -CDp obtained by isothermal titration calorimetry at 298 K in H<sub>2</sub>O. Bottom panel shows the integrated heat data fitted to a single-site binding model. Inset: Corresponding thermodynamic parameters and stoichiometry of binding.

polymer network are accessible to the guest molecules with relatively high association constant ( $5.29 \times 10^4 \text{ M}^{-1}$ ). We have obtained  $\Delta H = -19.75 \text{ kJ mol}^{-1}$ ,  $T\Delta S = 7.22 \text{ kJ mol}^{-1}$ , and calculated the Gibbs free energy,  $\Delta G$ , as  $-26.97 \text{ kJ mol}^{-1}$ . A negative value of  $\Delta H$  indicates that the interaction between 1AD and  $\beta$ -CDp is exothermic with a minor entropic contribution. Moreover, the complexation between 1AD and  $\beta$ -CDp is a spontaneous process as evidenced by the negative value of  $\Delta G$ . Formation of  $\beta$ -CDp/1AD inclusion complex is an enthalpically ( $|\Delta H| > |T\Delta S|$ ) driven process associated with the expulsion of high energy water molecules from the cavity as a part of the hydrophobic effect. Moreover, the reorganization of cavity/surface water molecules in  $\beta$ -CDp upon its complexation with 1AD along with the translational and conformational freedom available to the host and guest could explain the entropic contribution.<sup>35</sup>

Recently, Harada *et al.*<sup>36,37</sup> have shown that molecular-level association of  $\beta$ -CD with AD can drive macroscopic level self-assembly between semihard polymeric materials in the solid state. Moreover, they have also elegantly demonstrated that these materials show strong adhesive strength even after drying and self-healing effects using a minimal amount of H<sub>2</sub>O, thanks to the reversible nature of supramolecular interactions. We propose that such an adhesive effect can also be utilized in the context of silicon anodes, wherein broken electrode contacts during the volume expansion process can be restored during the volume

187 shrinkage, thus creating a dynamically cross-linked  
188 polymer network in a polar aprotic electrolyte such  
189 as ethylene carbonate with dipole moment of 4.9 D.<sup>38</sup>  
190 We propose that while the binding constant will be  
191 lower in ethylene carbonate compared to that in water,  
192 the rate of complexation will be much faster. The  
193 fast complexation will facilitate cross-linking of poly-  
194 mers *via* lyophobic forces arising from the increased  
195 solvent–solvent interactions due to the release of  
196 electrolyte molecules from the cavity upon complexa-  
197 tion. It is also important to note that a high local  
198 concentration of binder in the electrode matrix will  
199 provide an additional driving force for the host–guest  
200 interactions. In order to verify the ability of 6AD  
201 to cross-link  $\beta$ -CDp, we have carried out (see the SI,  
202 Figure S9) gelation experiments in  $H_2O$ . We dissolved  
203 premixed samples of 6AD and  $\beta$ -CDp in  $H_2O$  to reach  
204 the final concentrations of  $\beta$ -CDp ( $0.7\text{ g mL}^{-1}$ ) and 6AD  
205 ( $0.11\text{ g mL}^{-1}$ ), resulting in the formation of a highly  
206 viscous gel. Formation of the gel was verified by a  
207 simple tube inversion test (see the SI). Under identical  
208 experimental conditions, however,  $\beta$ -CDp ( $0.7\text{ g mL}^{-1}$ )  
209 alone formed only a slightly viscous liquid. We have  
210 also carried out (see SI, Figure S10) gelation experi-  
211 ments in organic media in order to mimic electrolyte  
212 conditions (ethylene carbonate (EC)/diethyl carbonate  
213 (DEC) = 1:1 vol %). We prepared the mixture of  $\beta$ -CDp  
214 ( $0.7\text{ g mL}^{-1}$ ) and  $\alpha$ -CDp ( $0.7\text{ g mL}^{-1}$ ) with 6AD  
215 ( $0.11\text{ g mL}^{-1}$ ) in DMSO (see the SI, Figure S10a) and  
216 electrolyte/DMSO (70/30 v%) mixture (see the SI,  
217 Figure S10b). We observed the formation of a viscous  
218 gel for  $\beta$ -CDp/6AD mixture in both DMSO and the  
219 electrolyte/DMSO mixture, whereas  $\alpha$ -CDp/6AD only  
220 formed a viscous liquid under the same conditions,  
221 indicating that gel formation in the case of the  $\beta$ -CDp/  
222 6AD mixture is solely driven by host–guest complexa-  
223 tion in organic media. In order to further prove the  
224 inclusion complex formation in the electrolyte, we pre-  
225 pared a mixture of both  $\beta$ -CDp/6AD and  $\alpha$ -CDp/6AD  
226 in the electrolyte. The resulting gel-like precipitate  
227 was filtered and washed extensively with electrolyte  
228 in order to remove free 6AD. The resulting solid was  
229 dried and analyzed using  $^1H$  NMR spectroscopy. Inter-  
230 interestingly, in the case of  $\alpha$ -CD, we did not observe any  
231 peaks associated with the adamantane protons of 6AD  
232 in the range of 2.1–1.5 ppm (Figure S11a), indicating  
233 that there is no complexation between  $\alpha$ -CDp and 6AD  
234 in the electrolyte. In the case of  $\beta$ -CDp, however, we  
235 observed the corresponding adamantane protons  
236 (Figure S11b), thus further proving that  $\beta$ -CDp can still  
237 form an inclusion complex with 6AD in the electrolyte.

238 To comprehensively understand the effect of dy-  
239 namic cross-linking based on host–guest interactions  
240 on the electrochemical performance of Si anodes, we  
241 carried out (see the SI) a series of galvanostatic mea-  
242 surements by using typical Li half-cells with Si loading  
243 amounts of  $\sim 0.8\text{ mg cm}^{-2}$ . It is noteworthy that bulky

hydroxyl side chains of  $\beta$ -CDp can reversibly accom-  
244 modate (see the SI, Figure S12) negligible amounts  
245 of lithium ions with reversible capacity less than  
246  $1\text{ mAh g}^{-1}$ .<sup>25</sup> We varied (Figure 3a, Table 1) the amount  
247 F3 of 6AD (0–25.5 wt %) while keeping the amount  $\beta$ -CDp  
248 T1 constant to determine the ideal composition between  
249 both components. Interestingly, we reached the best  
250 capacity retention of 90% after 150 cycles upon in-  
251 creasing the 6AD amount up to 8.5 wt %, which  
252 corresponds to 1:0.5 ( $\beta$ -CD/AD) stoichiometry. When  
253 we further increased the 6AD amount to 17 wt %  
254 (1:1 stoichiometry) and higher, the capacity reten-  
255 tion became worse (75% after 150 cycles). This result  
256 indicates that, unlike the solution state, not all of the  
257  $\beta$ -CD units are available for complexation in the binder  
258 due to their relatively strong hydrogen-bonding inter-  
259 actions with Si nanoparticles. It is important to note  
260 that the capacity retention at 17 wt % of 6AD is still  
261 higher than that of  $\beta$ -CDp alone. Beyond 1:1 stoichi-  
262 ometry, however, a further increase in the amount  
263 of 6AD to 25.5 wt % clearly impairs the capacity. This  
264 observation can be attributed to the negative impact  
265 of increasing the amount of noninteracting cross-  
266 linkers, suggesting the presence of an optimal point  
267 where the numbers of host and guest are matched.  
268 Above and below this point, the excess amount of  
269 either host or guest generates the dead occupancy in  
270 the electrode and deteriorates the cycling perfor-  
271 mance. The initial capacity increase of the electrodes  
272 incorporating 4.2–17.0 wt % 6AD could be attributed  
273 to cross-linked binder layer on Si surface, which could  
274 impede electrolyte uptake to Si. In contrast, the elec-  
275 trodes with 0 and 25.5 wt % have shown no initial  
276 capacity increase. As the 25.5% corresponds to 1:1.5  
277 ( $\beta$ -CD/AD) stoichiometry, excess cross-linker is anti-  
278 cipated to create paths within the binder layer for  
279 electrolyte uptake.  
280

In order to further verify that the origin of capacity  
281 enhancement is the host–guest interaction between  
282  $\beta$ -CD and AD, we also carried out control experiments  
283 using  $\alpha$ -CDp and  $\gamma$ -CDp. While  $\gamma$ -CDp can form very  
284 weak inclusion complexes with AD,  $\alpha$ -CDp cannot form  
285 an inclusion complex at all due to size/shape mis-  
286 match. As expected, all  $\alpha$ -,  $\beta$ -, and  $\gamma$ -CDp without any  
287 dynamic cross-linker exhibited comparable capacity  
288 retentions of 69%, 66%, and 54% after 150 cycles,  
289 respectively (Figure 3b). When we compare the elec-  
290 trochemical performance of  $\alpha$ -,  $\beta$ -, and  $\gamma$ -CDp at 8.5 wt  
291 % 6AD loading, the impact of dynamic cross-linking  
292 based on host–guest interactions becomes clearly  
293 visible. While  $\beta$ -CDp/6AD (8.5 wt %) showed capacity  
294 retention up to 90%, those of  $\alpha$ -CDp/6AD (8.5 wt %,  
295 no cross-linking) and  $\gamma$ -CDp/6AD (8.5 wt %, weak cross-  
296 linking) were found to be only 19 and 35%, respec-  
297 tively. Slightly higher capacity retention of  $\gamma$ -CDp/6AD  
298 can be explained by the formation of a weak inclusion  
299 complex.  
300

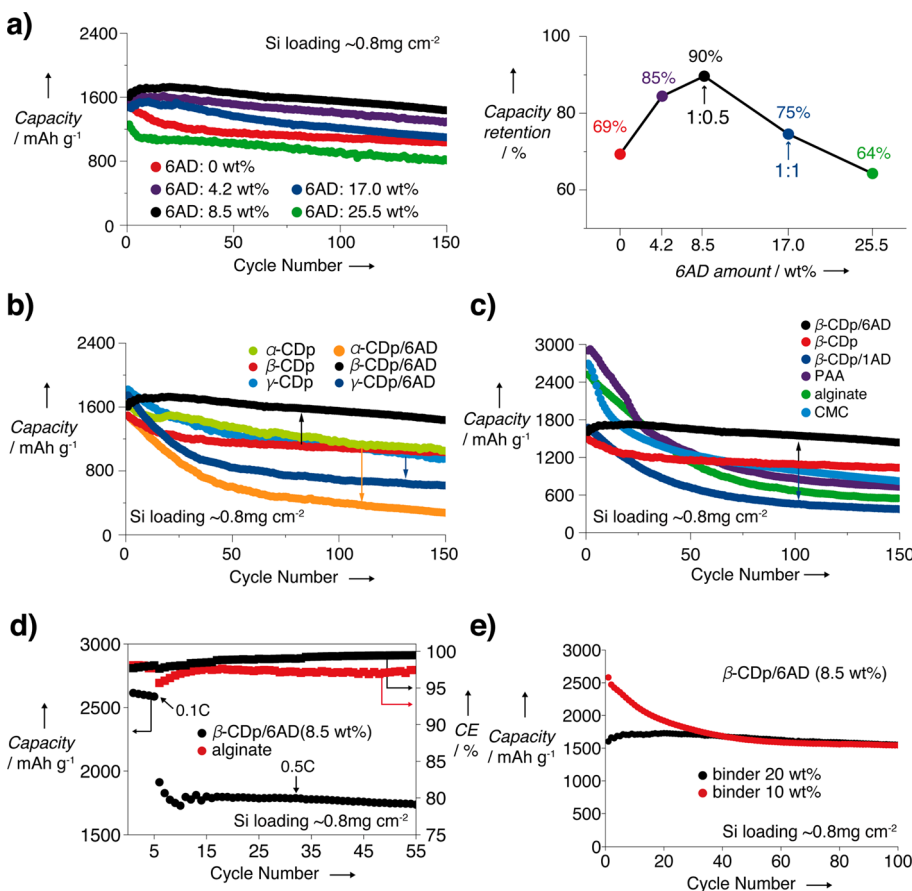


**Figure 3.** Electrochemical measurements of Si electrodes at 0.5C (1500 mA g<sup>-1</sup>). Except for a control electrode in (e), for all electrodes, the ratio of components was fixed as Si/SuperP/binder = 60:20:20 wt %. 6AD or 1AD was additionally added to these electrodes. Si mass loading = ~0.8 mg cm<sup>-2</sup>, electrolyte = 1 M LiPF<sub>6</sub> in EC/DEC = 1:1 v/v with 5 wt % FEC. Prior to the cycling data shown in this figure, all cells underwent one precycle at 0.1C (300 mA g<sup>-1</sup>) for stable SEI formation. (a) Cycling performance of Si electrode based on the different amounts of 6AD (0–25.5 wt %). (Right panel) Plot of capacity retention after 150 cycles with respect to increasing amount of 6AD to determine an optimal binder composition. (b) Comparison of cycling performance of Si electrode incorporating  $\alpha$ , $\beta$ , $\gamma$ -CDp alone and those with 8.5 wt % 6AD. (c) Comparison of cycling performance of Si electrode based on  $\beta$ -CDp/1AD to those based on  $\beta$ -CDp,  $\beta$ -CDp/6AD (guest loading: 8.5 wt %), PAA, alginate, and CMC. (d) Cycling performance and Coulombic efficiencies of Si electrode including  $\beta$ -CDp/6AD (8.5 wt %) and alginate. (e) Cycling performance of Si electrodes based on 10 and 20 wt % binder ( $\beta$ -CDp/6AD) with 6AD occupying 8.5 wt % of the binder. For the control electrode, the composition is Si/SuperP/binder = 60:30:10 wt %. All of the specific capacities in this work are based on the weight of Si only.

**TABLE 1. Capacity, Capacity Retention, Inclusion Strength, and Cross-Linking Strength of the Mixture of Three Different CDp and Guest Molecules**

| binder        | linker | ICE <sup>a</sup> (%) | capacity retention <sup>b</sup> (%) | inclusion <sup>c</sup> | cross-linking <sup>c</sup> |
|---------------|--------|----------------------|-------------------------------------|------------------------|----------------------------|
| $\beta$ -CDp  |        | 78                   | 69                                  | no                     | no                         |
|               | 6AD    | <b>84</b>            | <b>90</b>                           | <b>strong</b>          | <b>strong</b>              |
|               | 1AD    | 83                   | 23                                  | strong                 | no                         |
| $\alpha$ -CDp |        | 79                   | 64                                  | no                     | no                         |
|               | 6AD    | 84                   | 19                                  | no                     | no                         |
|               | 1AD    | 87                   | 29                                  | no                     | no                         |
| $\gamma$ -CDp |        | 79                   | 53                                  | no                     | no                         |
|               | 6AD    | 85                   | 35                                  | weak                   | weak                       |
|               | 1AD    | 84                   | 23                                  | weak                   | no                         |

<sup>a</sup>Initial coulombic efficiency (ICE). <sup>b</sup>Capacity and its retention are based on the value at the 150th cycle. 1AD and 6AD amounts are 8.5 wt %. <sup>c</sup>These are determined from the typical association constants.

We have also shown that  $\beta$ -CDp/6AD performs much better when compared to conventional linear

binders, including alginate, PAA, and CMC (Figure 3c). Under the same experimental conditions, all three linear binders showed rapid capacity decay, reaching only 21.7%, 25.2%, and 30.5% capacity retentions after 150 cycles. These results signify that the dynamic cross-linking based on host–guest interactions is responsible for the enhanced cycling performance of  $\beta$ -CDp/6AD. These findings were further supported by comparing the cycling performance of  $\beta$ -CDp/6AD with  $\beta$ -CDp/1AD at 8.5 wt % guest loading (Figure 3c). Compared to the 90% capacity retention of  $\beta$ -CDp/6AD,  $\beta$ -CDp/1AD exhibited far inferior performance (23% capacity retention), thus indicating that host–guest interactions need to be coupled with dendritic cross-linking in order to better preserve the electrode film integrity. These results are indeed consistent with natural and artificial supramolecular systems, wherein an increasing number of noncovalent interactions with positive cooperativity contribute further to the stability

of resulting supramolecular assembly. When measured at 0.5C following the first five cycles at 0.1C, the CE of  $\beta$ -CDp/6AD reached 99.5% after 55 cycles (Figure 3d). This value is higher than that (97.5%) of the alginate case after the same number of cycles. When the binder content decreased to 10 wt %, a capacity of 1542.6 mAh g<sup>-1</sup> was observed after 100 cycles (Figure 3e), which is similar to 1550.7 mAh g<sup>-1</sup> of the 20 wt % case. This value is indeed higher than those (860.7, 667.5, and 997.1 mAh g<sup>-1</sup>) of the PAA, alginate, and CMC cases after the same number of cycles, so the given dynamic cross-linking concept is valid in the lowered binder content. The initial capacity decay of the 10 wt % case is attributed to a rearrangement process of the binder until the overall binder network becomes stabilized. The higher initial capacities of the 10 wt % case originates from the lowered resistance after decreasing the binder content. Based on this understanding, we expect that a constant capacity measurement can be applied to the initial period of cycles to deliver persistent capacities.

We have also tested (Figure S13 and S14)  $\alpha$ -CDp/1AD (8.5 wt %) and  $\gamma$ -CDp/1AD (8.5 wt %), both of which exhibited very low capacity retentions of 29% and 23% after 150 cycles, respectively (Figure S14). It was also consistently observed (Table 1) that the initial Coulombic efficiency (ICE) increases for all  $\alpha$ -,  $\beta$ -, and  $\gamma$ -CDp upon addition of 6AD and 1AD, which is attributed to the fact that the improved electrode integrity by the dynamic cross-linking results in a lesser degree of electrolyte decomposition. More electrochemical and FT-IR results of  $\beta$ -CDp/6AD are available in Figures S15–17.

A morphology inspection using scanning electron microscopy (SEM) (Figure 4) reconfirmed the importance of appropriate host–guest interaction. Even after 150 cycles,  $\beta$ -CDp/6AD (8.5 wt %) showed clear morphologies of Si nanoparticles without any micro-cracks, implying that the dynamic cross-linking with the right host–guest interactions enables SEI layers to remain stable throughout the cycling (Figure 4b). In sharp contrast,  $\alpha$ - and  $\gamma$ -CDp/6AD with the same 6AD content lost the stability of SEI layers to a level that Si nanoparticles are fully buried underneath the SEI layers. In order to further demonstrate the ability of a dynamic cross-linker to tolerate the volume expansion and restore electrode morphology, that is the self-healing effect, we have carried out (Figure S18) an

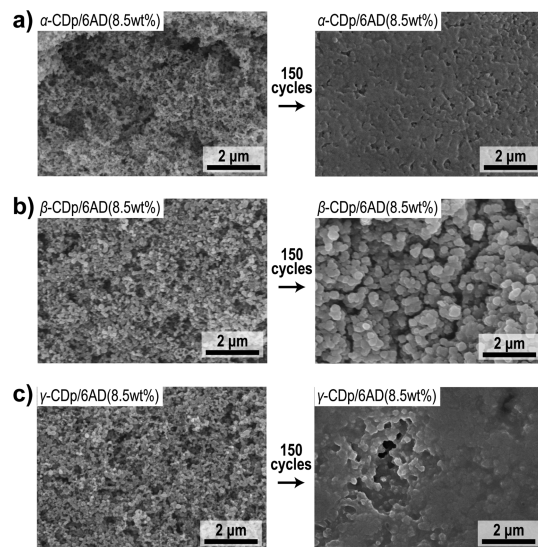


**Figure 4.** Morphology of Si electrode surfaces before and after 150 cycles containing (a)  $\alpha$ -CDp/6AD (8.5 wt %), (b)  $\beta$ -CDp/6AD (8.5 wt %), and (c)  $\gamma$ -CDp/6AD (8.5 wt %).

additional SEM analysis. We visualized the same area of the electrode after the first cycle and second cycle. During the first charge/discharge process, the electrode undergoes the largest volume expansion along with the formation of SEI layer, leading to cracking of the electrode. However, after the subsequent cycle, generated cracks closed up thanks to the dynamic nature of host–guest interactions.

## CONCLUSIONS

We have introduced a new binder concept for silicon anodes, “dynamic crosslinking”, which is based on supramolecular host–guest interactions. The dynamic cross-linking allows for intimate Si–binder interactions, structural stability of electrode film, and controlled SEI formation, leading to superior cycling performance to that of either of host or guest alone as well as most of the other conventional binders at the same level of active material loading. Importantly, the host–guest interaction with the molecular-level sensitivity is translated directly to the cycling performance of silicon anodes. Considering the vast number of host–guest complexes available in the literature, our findings based on supramolecular interactions will bring a whole new perspective on binder design for high capacity electrode materials suffering from large volume expansion.

## METHODS

**General Methods.** Diisopropylethylamine (DIEA) was purchased from Sigma-Aldrich, and *o*-(benzotriazol-1-yl)-*N,N,N',N'*-tetramethyluronium tetrafluoroborate (TBTU) was purchased from Bachem. 1,2-Bis(2-aminoethoxy)ethane was purchased from Tokyo Chemical Industry Co.. Sodium hydroxide and hydrochloric acid were purchased from Samchun (Korea).  $\alpha$ - and  $\beta$ -CDp were

purchased from Cyclolab.  $\gamma$ -CDp and alginic acid sodium salt was purchased from Sigma-Aldrich. Si nanoparticle powder (diameter: ~ 50 nm, Nanostructured & Amorphous Materials) was used as an active material, and SuperP was used as a conducting agent. Synthetic procedures of the guests are described in the Supporting Information in detail. <sup>1</sup>H NMR spectra were recorded on a Bruker AVANCE 300 spectrometer using residual solvent peaks as

411 an internal standard ( $\text{CDCl}_3$ :  $\delta$  7.26). Fourier transform infrared  
 412 (FT-IR) spectra were recorded using a Shimadzu FT-IR spectrometer  
 413 (IRTracer-100). Isothermal titration calorimetry (ITC) experiments  
 414 were carried out using a MicroCal VP-ITC calorimeter.

415 **Preparation of Electrodes.** Si nanoparticle powder (diameter:  
 416 ~ 50 nm, Nanostructured & Amorphous Materials) was used as an  
 417 active material, and SuperP was used as a conducting agent.  
 418 For cell fabrication, 2032 type stainless steel coin cells were used.  
 419 Li metal were arranged as both reference and counter electrodes, and polyethylene films were used as a separator. Lithium  
 420 hexafluorophosphate ( $\text{LiPF}_6$ ) (1 M) dissolved in ethylene carbonate  
 421 (EC)/diethyl carbonate (DEC) = 1:1 vol % with 5 wt %  
 422 fluoroethylene carbonate (FEC) was used as an electrolyte. All  
 423 cell assembly procedures were performed in an Ar-filled glovebox.  
 424 For electrochemical measurements, the cells were galvanostatically scanned by using a battery cycler (PNE Solutions).  
 425 All cells were aged before any operations for at least 2 h and  
 426 underwent one formation cycle at 0.1C (300 mA g<sup>-1</sup>), followed  
 427 by subsequent cycles at 0.5C. The capacity retention was cal-  
 428 culated on the basis of the capacity of the first cycle in the  
 429 subsequent cycles (excluding the precycling). All cycles were  
 430 scanned in the voltage range of 0–1.0 V vs Li/Li<sup>+</sup>. Cyclic  
 431 voltammetry of Si electrode based on  $\beta$ -CDp/6AD was per-  
 432 formed using a battery cycler (WonATech) at 30  $\mu\text{V s}^{-1}$  in the  
 433 voltage range of 0–1.5 V vs Li/Li<sup>+</sup> at 25 °C.

434 **Scanning Electron Microscopy Measurement.** After 150 cycles,  
 435 coin cells were disassembled, and the tested Si electrodes were  
 436 then fully rinsed with propylene carbonate (PC). These washed  
 437 electrodes were predried at room temperature in an Ar glove-  
 438 box for 2 h and then completely dried in a vacuum chamber  
 439 for 2 h. In order to visualize surface morphology of Si elec-  
 440 trode, 9 nm of Pt was sputtered on each sample, and FE-SEM  
 441 (field-emission scanning electron microscopy, Hitachi) was used  
 442 for visualization.

443 **Conflict of Interest:** The authors declare no competing  
 444 financial interest.

445 **Supporting Information Available:** The Supporting Informa-  
 446 tion is available free of charge on the ACS Publications website  
 447 at DOI: 10.1021/acsnano.5b05030.

448 **Synthesis details, additional spectroscopic data, gelation  
 449 experiments and electrochemical characterization data (PDF)**

450 **Acknowledgment.** A.C. acknowledges the support from the  
 451 Basic Science Research Program through the National Research  
 452 Foundation of Korea (NRF) funded by the Ministry of Science,  
 453 ICT & Future Planning (2013R1A1A1012282). J.W.C. acknowl-  
 454 edges support through the National Research Foundation of  
 455 Korea (NRF) grant funded by the Korean government (MEST)  
 456 (NRF-2012-R1A2A1A01011970). This work was also made possible  
 457 by a NPPR grant (NPPR 7-301-2-126) from the Qatar National  
 458 Research Fund (a member of Qatar Foundation). This work  
 459 was also partially supported by a National Research Foundation  
 460 of Korea (NRF) grant funded by the Korean government (MEST)  
 461 (NRF-2014R1A4A1003712 and BK21 PLUS program). The man-  
 462 uscript was written through contributions of all authors. All authors  
 463 have given approval to the final version of the manuscript.

## 466 REFERENCES AND NOTES

1. Weydanz, W. J.; Wohlfahrt-Mehrens, M.; Huggins, R. A. A Room Temperature Study of the Binary Lithium–Silicon and the Ternary Lithium–Chromium–Silicon System for Use in Rechargeable Lithium Batteries. *J. Power Sources* **1999**, *81*–82, 237–242.
2. Esmanski, A.; Ozin, G. A. Silicon Inverse-Opal-Based Macroporous Materials as Negative Electrodes for Lithium Ion Batteries. *Adv. Funct. Mater.* **2009**, *19*, 1999–2010.
3. Yin, Y.-X.; Xin, S.; Wan, L.-J.; Li, C.-J.; Guo, Y.-G. Electrospray Synthesis of Silicon/Carbon Nanoporous Microspheres as Improved Anode Materials for Lithium-Ion Batteries. *J. Phys. Chem. C* **2011**, *115*, 14148–14154.
4. Zhou, X.; Yin, Y.-X.; Wan, L.-J.; Guo, Y.-G. Facile Synthesis of Silicon Nanoparticles Inserted into Graphene Sheets as Improved Anode Materials for Lithium-Ion Batteries. *Chem. Commun.* **2012**, *48*, 2198–2200.
5. Jung, D. S.; Ryou, M. H.; Sung, Y. J.; Park, S. B.; Choi, J. W. Recycling Rice Husks for High-Capacity Lithium Battery Anodes. *Proc. Natl. Acad. Sci. U. S. A.* **2013**, *110*, 12229–12234.
6. Wang, B.; Li, X.; Luo, B.; Hao, L.; Zhou, M.; Zhang, X.; Fan, Z.; Zhi, L. Approaching the Downsizing Limit of Silicon for Surface-Controlled Lithium Storage. *Adv. Mater.* **2015**, *27*, 1526–1532.
7. Wang, B.; Li, X.; Qiu, T.; Luo, B.; Ning, J.; Li, J.; Zhang, X.; Liang, M.; Zhi, L. High Volumetric Capacity Silicon-Based Lithium Battery Anodes by Nanoscale System Engineering. *Nano Lett.* **2013**, *13*, 5578–5584.
8. Wang, B.; Li, X.; Zhang, X.; Luo, B.; Jin, M.; Liang, M.; Dayeh, S. A.; Picraux, S. T.; Zhi, L. Adaptable Silicon–Carbon Nanocables Sandwiched between Reduced Graphene Oxide Sheets as Lithium Ion Battery Anodes. *ACS Nano* **2013**, *7*, 1437–1445.
9. Wilson, A. M.; Zank, G.; Eguchi, K.; Xing, W.; Dahn, J. R. Pyrolysed Silicon-Containing Polymers as High Capacity Anodes for Lithium-Ion Batteries. *J. Power Sources* **1997**, *68*, 195–200.
10. Morita, T.; Takami, N. Nano Si Cluster-SiOx-C Composite Material as High-Capacity Anode Material for Rechargeable Lithium Batteries. *J. Electrochem. Soc.* **2006**, *153*, A425–A430.
11. Lee, J.-I.; Lee, K. T.; Cho, J.; Kim, J.; Choi, N.-S.; Park, S. Chemical-Assisted Thermal Disproportionation of Porous Silicon Monoxide into Silicon-Based Multicomponent Systems. *Angew. Chem.* **2012**, *124*, 2821–2825.
12. Choi, S.; Jung, D. S.; Choi, J. W. Scalable Fracture-Free SiOC Glass Coating for Robust Silicon Nanoparticle Anodes in Lithium Secondary Batteries. *Nano Lett.* **2014**, *14*, 7120–7125.
13. Liu, W.-R.; Yen, Y.-C.; Wu, H.-C.; Winter, M.; Wu, N.-L. Nano-Porous SiO<sub>x</sub>/Carbon Composite Anode for Lithium-Ion Batteries. *J. Appl. Electrochem.* **2009**, *39*, 1643–1649.
14. Mazouzi, D.; Lestriez, B.; Roué, L.; Guyomard, D. Silicon Composite Electrode with High Capacity and Long Cycle Life. *Electrochim. Solid-State Lett.* **2009**, *12*, A215–A218.
15. Bridel, J. S.; Azaïs, T.; Morcrette, M.; Tarascon, J. M.; Larcher, D. Key Parameters Governing the Reversibility of Si/Carbon/Cmc Electrodes for Li-Ion Batteries. *Chem. Mater.* **2010**, *22*, 1229–1241.
16. Magasinski, A.; Zdyrko, B.; Kovalenko, I.; Hertzberg, B.; Burtovyy, R.; Huebner, C. F.; Fuller, T. F.; Luzinov, I.; Yushin, G. Toward Efficient Binders for Li-Ion Battery Si-Based Anodes: Polyacrylic Acid. *ACS Appl. Mater. Interfaces* **2010**, *2*, 3004–3010.
17. Kovalenko, I.; Zdyrko, B.; Magasinski, A.; Hertzberg, B.; Milicev, Z.; Burtovyy, R.; Luzinov, I.; Yushin, G. A Major Constituent of Brown Algae for Use in High-Capacity Li-Ion Batteries. *Science* **2011**, *334*, 75–79.
18. Koo, B.; Kim, H.; Cho, Y.; Lee, K. T.; Choi, N. S.; Cho, J. A Highly Cross-Linked Polymeric Binder for High-Performance Silicon Negative Electrodes in Lithium Ion Batteries. *Angew. Chem., Int. Ed.* **2012**, *51*, 8762–7.
19. Song, J.; Zhou, M.; Yi, R.; Xu, T.; Gordoin, M. L.; Tang, D.; Yu, Z.; Regula, M.; Wang, D. Interpenetrated Gel Polymer Binder for High-Performance Silicon Anodes in Lithium-Ion Batteries. *Adv. Funct. Mater.* **2014**, *24*, 5904–5910.
20. Kwon, T.-W.; Jeong, Y. K.; Lee, I.; Kim, T.-S.; Choi, J. W.; Coskun, A. Systematic Molecular-Level Design of Binders Incorporating Meldrum's Acid for Silicon Anodes in Lithium Rechargeable Batteries. *Adv. Mater.* **2014**, *26*, 7979–7985.
21. Liu, G.; Xun, S.; Vukmirovic, N.; Song, X.; Olalde-Velasco, P.; Zheng, H.; Battaglia, V. S.; Wang, L.; Yang, W. Polymers with Tailored Electronic Structure for High Capacity Lithium Battery Electrodes. *Adv. Mater.* **2011**, *23*, 4679–4683.
22. Park, S.-J.; Zhao, H.; Ai, G.; Wang, C.; Song, X.; Yuca, N.; Battaglia, V. S.; Yang, W.; Liu, G. Side-Chain Conducting and Phase-Separated Polymeric Binders for High-Performance Silicon Anodes in Lithium-Ion Batteries. *J. Am. Chem. Soc.* **2015**, *137*, 2565–2571.
23. Jeena, M. T.; Lee, J.-I.; Kim, S. H.; Kim, C.; Kim, J.-Y.; Park, S.; Ryu, J.-H. Multifunctional Molecular Design as an Efficient

- 558 Polymeric Binder for Silicon Anodes in Lithium-Ion Batteries. *ACS Appl. Mater. Interfaces* **2014**, *6*, 18001–18007.
- 559
- 560 24. Murase, M.; Yabuuchi, N.; Han, Z.-J.; Son, J.-Y.; Cui, Y.-T.; Oji, H.; Komaba, S. Crop-Derived Polysaccharides as Binders for High-Capacity Silicon/Graphite-Based Electrodes in Lithium-Ion Batteries. *ChemSusChem* **2012**, *5*, 2307–2311.
- 561
- 562 25. Jeong, Y. K.; Kwon, T.-w.; Lee, I.; Kim, T.-S.; Coskun, A.; Choi, J. W. Hyperbranched B-Cyclodextrin Polymer as an Effective Multidimensional Binder for Silicon Anodes in Lithium Rechargeable Batteries. *Nano Lett.* **2014**, *14*, 864–870.
- 563
- 564 26. Ryou, M. H.; Kim, J.; Lee, I.; Kim, S.; Jeong, Y. K.; Hong, S.; Ryu, J. H.; Kim, T. S.; Park, J. K.; Lee, H.; Choi, J. W. Mussel-Inspired Adhesive Binders for High-Performance Silicon Nanoparticle Anodes in Lithium-Ion Batteries. *Adv. Mater.* **2013**, *25*, 1571–1576.
- 565
- 566 27. Chen, D.; Yi, R.; Chen, S.; Xu, T.; Gordin, M. L.; Wang, D. Facile Synthesis of Graphene–Silicon Nanocomposites with an Advanced Binder for High-Performance Lithium-Ion Battery Anodes. *Solid State Ionics* **2014**, *254*, 65–71.
- 567
- 568 28. Jeong, Y. K.; Kwon, T.-w.; Lee, I.; Kim, T.-S.; Coskun, A.; Choi, J. W. Millipede-Inspired Structural Design Principle for High Performance Polysaccharide Binders in Silicon Anodes. *Energy Environ. Sci.* **2015**, *8*, 1224.
- 569
- 570 29. Wang, C.; Wu, H.; Chen, Z.; McDowell, M. T.; Cui, Y.; Bao, Z. Self-Healing Chemistry Enables the Stable Operation of Silicon Microparticle Anodes for High-Energy Lithium-Ion Batteries. *Nat. Chem.* **2013**, *5*, 1042–8.
- 571
- 572 30. Chen, Z.; Wang, C.; Lopez, J.; Lu, Z.; Cui, Y.; Bao, Z. High-Areal-Capacity Silicon Electrodes with Low-Cost Silicon Particles Based on Spatial Control of Self-Healing Binder. *Adv. Energy Mater.* **2015**, *10.1002/aenm.201401826*.
- 573
- 574 31. Connors, K. A. The Stability of Cyclodextrin Complexes in Solution. *Chem. Rev.* **1997**, *97*, 1325–1357.
- 575
- 576 32. Siegel, B.; Breslow, R. Lyophobic Binding of Substrates by Cyclodextrins in Nonaqueous Solvents. *J. Am. Chem. Soc.* **1975**, *97*, 6869–6870.
- 577
- 578 33. Renard, E.; Deratani, A.; Volet, G.; Sebille, B. Preparation and Characterization of Water Soluble High Molecular Weight B-Cyclodextrin-Epichlorohydrin Polymers. *Eur. Polym. J.* **1997**, *33*, 49–57.
- 579
- 580 34. Inoue, Y.; Hakushi, T.; Liu, Y.; Tong, L. H.; Shen, B. J.; Jin, D. S. Thermodynamics of Molecular Recognition by Cyclodextrins. 1. Calorimetric Titration of Inclusion Complexation of Naphthalenesulfonates with Alpha-Cyclodextrin, Beta-Cyclodextrin, and Gamma-Cyclodextrin - Enthalpy Entropy by Compensation. *J. Am. Chem. Soc.* **1993**, *115*, 475–481.
- 581
- 582 35. Daoud-Mahammed, S.; Couvreur, P.; Bouchemal, K.; Chéron, M.; Lebas, G.; Amiel, C.; Gref, R. Cyclodextrin and Polysaccharide-Based Nanogels: Entrapment of Two Hydrophobic Molecules, Benzophenone and Tamoxifen. *Biomacromolecules* **2009**, *10*, 547–554.
- 583
- 584 36. Kakuta, T.; Takashima, Y.; Sano, T.; Nakamura, T.; Kobayashi, Y.; Yamaguchi, H.; Harada, A. Adhesion between Semihard Polymer Materials Containing Cyclodextrin and Adamantanane Based on Host–Guest Interactions. *Macromolecules* **2015**, *48*, 732–738.
- 585
- 586 37. Harada, A.; Kobayashi, R.; Takashima, Y.; Hashidzume, A.; Yamaguchi, H. Macroscopic Self-Assembly through Molecular Recognition. *Nat. Chem.* **2011**, *3*, 34–37.
- 587
- 588 38. Payne, R.; Theodorou, I. E. Dielectric Properties and Relaxation in Ethylene Carbonate and Propylene Carbonate. *J. Phys. Chem.* **1972**, *76*, 2892–2900.
- 589
- 590
- 591
- 592
- 593
- 594
- 595
- 596
- 597
- 598
- 599
- 600
- 601
- 602
- 603
- 604
- 605
- 606
- 607
- 608
- 609
- 610
- 611
- 612
- 613
- 614
- 615
- 616
- 617
- 618
- 619